Dirac and Weyl Superconductors in Three Dimensions

Shengyuan A. Yang,[1] Hui Pan,[2] and Fan Zhang[3,4,5,*]

[1]*Engineering Product Development, Singapore University of Technology and Design, Singapore 138682, Singapore*
[2]*Department of Physics, Beihang University, Beijing 100191, China*
[3]*Department of Physics, University of Texas at Dallas, Richardson, Texas 75080, USA*
[4]*Department of Physics and Astronomy, University of Pennsylvania, Philadelphia, Pennsylvania 19104, USA*
[5]*Kavli Institute for Theoretical Physics, University of California, Santa Barbara, California 93106, USA*

We introduce the concept of three-dimensional Dirac (Weyl) superconductors (SC), which have protected bulk fourfold (twofold) nodal points and surface Majorana arcs at zero energy. We provide a sufficient criterion for realizing them in centrosymmetric SCs with odd-parity pairing and mirror symmetry. Pairs of Dirac nodes appear in a mirror-invariant plane when the mirror winding number is nontrivial. Breaking mirror symmetry may gap Dirac nodes producing a topological SC. Each Dirac node evolves to a nodal ring when inversion-gauge symmetry is broken, whereas it splits into a pair of Weyl nodes when, and only when, time-reversal symmetry is broken.

Topological states of matter have attracted significant attention since the discovery of topological insulators [1]. The idea of topological classification was soon generalized to superconductors (SC) which have energy gaps for quasiparticles [2]. Interestingly, topological phases also exist for systems without energy gaps. Graphene and its *ABC* stacked cousins are examples of two-dimensional (2D) semimetals [3,4], in which their Fermi surfaces consist of isolated points that are protected by the chiral (sublattice) symmetries. Indeed, the constant energy surfaces of these graphene few-layers have winding numbers set by the number of layers. Recently, the topological semimetal concept has been extended to three dimensions (3D). Unlike the critical point between 3D trivial and topological insulators with inversion symmetry, the fourfold degenerate Fermi points in 3D Dirac semimetals [5–12] are protected by crystalline symmetries. When an essential symmetry is broken, a Dirac semimetal, both in 2D and 3D, may become a topological or a trivial insulator. Moreover, a Dirac point may split into Weyl points when inversion or time-reversal symmetry (TRS) is broken, and the Dirac semimetal becomes a Weyl semimetal. A pair of 3D Weyl points [13–19] is protected by Chern numbers ± 1 of the constant energy surfaces enclosing either Weyl node, leading to a surface Fermi arc. In contrast, a 3D Dirac semimetal may or may not have a surface Fermi arc. Nevertheless, it is generally not an easy task to pin the Fermi energy exactly at the nodal points in semimetals.

Nodal phases are common for unconventional SCs. One may naturally wonder whether there also exist Dirac SCs in 3D. Remarkably enough, in this Letter, we discover a sufficient criterion for their realization. We will discuss the topological protection of Dirac nodes in 3D SCs and their surface consequences under various symmetry breaking scenarios. The latter provides an alternative to the realization of 3D Weyl SCs [20–25].

In the Bogliubov–de Gennes (BdG) description of SCs, the particle-hole redundancy leads to a natrual half-filling and an intrinsic particle-hole symmetry (PHS). Compared to the cases of semimetals, the former feature simplifies our task to focus on the nodal points at zero energy, whereas the latter feature poses an additional symmetry constraint which plays intriguing roles in stabilizing the nodes. Specifically, we find that a 3D Dirac SC can be realized in a nodal phase of a centrosymmetric SC with odd-parity pairing and mirror symmetry. Pairs of Dirac nodes would appear in a mirror-invariant plane when the mirror winding number [26,27] is nontrivial. Each Dirac node is protected locally by the combination of mirror symmetry, TRS, and an inversion-gauge symmetry which we will introduce in a short while.

Breaking any symmetry destroys the Dirac nodes: (i) breaking mirror symmetry may fully gap the nodes producing a topological SC; (ii) breaking inversion-gauge symmetry extends each Dirac node to a robust nodal ring; (iii) a Dirac node may split into a pair of Weyl nodes when and only when TRS is broken. These evolutions of bulk Dirac nodes and the corresponding deformations of surface Majorana arcs are summarized in Fig. 2. Our physics might be realized in the nodal phase of $Cu_x Bi_2 Se_3$, which at least serves as a concrete example to illustrate the essential physics we will present.

Our analysis starts from the Fu-Berg BdG mean-field model [28] describing the SC states of $Cu_x Bi_2 Se_3$:

$$H = [v(\boldsymbol{k} \times \boldsymbol{s}) \cdot \hat{z}\sigma_z + v_z k_z \sigma_y + m\sigma_x - \mu]\tau_z + \Delta\tau_x, \quad (1)$$

where the Pauli matrices $\boldsymbol{\sigma}$, $\boldsymbol{s}$, and $\boldsymbol{\tau}$ act on the orbital, spin, and Nambu spaces, respectively. For each orbital we have chosen the basis as $(c_{\boldsymbol{k}\uparrow}, c_{\boldsymbol{k}\downarrow}, c_{-\boldsymbol{k}\downarrow}^\dagger, -c_{-\boldsymbol{k}\uparrow}^\dagger)^T$. The τ_z-term
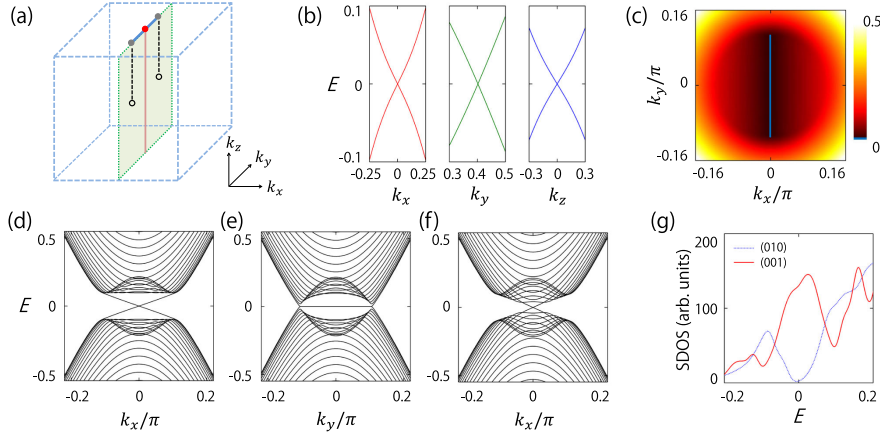
FIG. 1 (color online). Features of a 3D Dirac SC. (a) Two Dirac nodes (black dots) located in the (shaded) mirror invariant plane. The nontrivial mirror winding number of the $k_x = k_y = 0$ (pink) line protects the nodes and dictates the presence of a Majorana arc (blue line) with a Majorana Kramers pair (red dot) on the (001) surface. (b) Linear energy dispersions around one Dirac node from our tight binding calculations [33]; each band is doubly degenerate because of TRS and inversion-gauge symmetry. (c)–(e) Band structures of a (001) slab. The blue color in (c) corresponds to zero energy. (f) Band structures of a (010) slab. (g) Surface density of states for (001) and (010) surfaces.

describes the normal state near Γ point, with its form determined [29,30] by the inversion ($\mathcal{P} = \sigma_x$) symmetry, the mirror ($\mathcal{M} = -is_x$) symmetry, i.e.,

$$\mathcal{M}H(k_x, k_y, k_z)\mathcal{M}^{-1} = H(-k_x, k_y, k_z), \qquad (2)$$

and the $\mathcal{C}_3(\hat{z})$ symmetry of the $Cu_xBi_2Se_3$ crystal. $\hat{z}$ is the quintuple-layer normal, m is the normal state band gap, and μ is the chemical potential. The pairing term Δ can be classified [28] according to the representations of the crystal point group D_{3d}. The existence of mirror symmetry requires [26] the winding number to vanish for any fully gapped 3D SC with TRS. Indeed Fu and Berg have shown [28] that the topological state ($\Delta \sim \sigma_y s_z$) breaks the mirror symmetry whereas the states respecting the symmetry are either trivial ($\Delta \sim I$ or σ_x) or nodal. Our focus will be on the nodal phase with $\Delta \sim \sigma_y s_x$.

Under inversion the normal state has even parity whereas the pairing $\sigma_y s_x \tau_x$ has odd parity, yet the Hamiltonian (1) still has an inversion-gauge symmetry, i.e.,

$$\tau_z \mathcal{P}H(\boldsymbol{k})\mathcal{P}^{-1}\tau_z = H(-\boldsymbol{k}). \qquad (3)$$

We observe that in the mirror invariant plane with $k_x = 0$, the nodal points are located away from the time-reversal and mirror invariant line $k_y = 0$. Indeed, along this special line, the BdG Hamiltonian (1) reduces to

$$H = (v_z k_z \sigma_y + m\sigma_x - \mu)\tau_z + \Delta\sigma_y s_x \tau_x, \qquad (4)$$

the spectrum of which is fully gapped as long as the pair potential Δ is nonzero. It is easy to verify that Eq. (4) is adiabatically connected to the case for $m = \mu = 0$ (by first letting $m \to 0$ then $\mu \to 0$) described by

$$\bar{H} = v_z k_z \sigma_y \tau_z + \Delta\sigma_y s_x \tau_x, \qquad (5)$$

where both σ_y and s_x are good quantum numbers with eigenvalues ± 1. Now consider the interface between a 1D system described by Eq. (5) and the vacuum. The trivial vacuum is adiabatically connected to a pure s-wave SC and thus can be modeled by $v_z k_z \sigma_y \tau_z + \Delta_s \tau_x$, with $\Delta_s \to \infty$ and $\Delta_s \cdot \Delta > 0$ [29,31]. One recognizes that out of the four boundary problems with $\sigma_y = \pm 1$ and $s_x = \pm 1$, there are two copies of Jackiw-Rebbi problem [32]: i.e., one with $\sigma_y = -1$ and $s_x = 1$ and the other with $\sigma_y = 1$ and $s_x = -1$. Each Jackiw-Rebbi problem has a zero-energy bound state localized at the surface [29]. Due to the TRS and PHS, these two zero modes form a Majorana Kramers pair [31] at the top surface Brillouin zone (BZ) center, as sketched in Fig. 1(a). Moreover, across the center there exists a Majorana Kramers arc connecting the two surface projected nodal points.

To visualize the Dirac nodes and their surface consequences more clearly, we numerically calculate the energy spectrum for a (001) slab terminated by vacuum, using a layered hexagonal lattice model [34]. As shown in Figs. 1(b)–1(e), the two surface projected nodal points are located in the $k_x = 0$ line with finite k_y values; there is a flat surface arc connecting the projected nodal points; the arc is doubly degenerate and hosts a Majorana Kramers pair at its center. (We note by passing that for another nodal phase with $\Delta \sim \sigma_z$ ($\Delta \sim \sigma_y s_y$) in Ref. [28], two Dirac nodes appear in the $k_x = 0$ ($k_y = 0$) mirror invariant plane and align in the k_z (k_x) axis. Similar surface consequences also apply to these two phases.)

Remarkably, the presence and the flatness of Majorana Kramers arc in Fig. 1 are not accidental and indeed protected by the mirror symmetry and TRS, as we explain now. Consider the mirror invariant plane ($k_x = 0$) with a pair of nodal points at $k_y = \pm k_n$. In this plane, two mirror subspaces ($s_x = \pm$) decouple and are related by TRS and PHS. Both TRS and PHS are broken in each mirror subspace, yet the chiral symmetry, i.e., the product of TRS and PHS, is still

respected. For any fully gapped loop l in this plane, the presence of chiral symmetry allows the definitions of total and mirror winding numbers [26] as follows:

$$\gamma_{t,m} = \frac{1}{2\pi} \oint_l (\mathcal{A}_{k+} \pm \mathcal{A}_{k-}) \cdot d\mathbf{k}, \qquad (6)$$

where $\mathcal{A}_{k\pm}$ is the Berry connection of the negative energy bands in the $s_x = \pm$ mirror subspace. Explicit calculations show that $\gamma_m = 1$ [35] and $\gamma_t = 0$ for Eq. (4), which dictates the presence of a Majorana Kramers pair [31] at the surface BZ center. In the $k_x = 0$ plane, the states in $k_y = a$ loops with $|a| < k_n$ and with $|a| > k_n$ are adiabatically connected to the state of Eq. (4) and to the vacuum state [36], respectively. Hence in the former case $\gamma_m = 1$ whereas in the latter case $\gamma_m = 0$. Equivalently, $\gamma_m = 1(-1)$ for any loop enclosing the $k_y = k_n(-k_n)$ nodal point whereas $\gamma_m = 0$ for any loop enclosing both or neither nodal points. The nontrivial γ_m has two important consequences.

First, the nodal points must exist in the mirror invariant plane. Suppose that there is no nodal point in the plane, then the presence of chiral symmetry requires that both the total and the mirror Berry curvatures must vanish [26], leading to a contradicting result $\gamma_m(0) = \gamma_m(\pi)$ via Stokes' theorem. Therefore, the derived difference in γ_m implies the presence of a pair of nodal points in the plane. Out of the plane, the absence of mirror invariance implies gap opening. Figure 1(b) shows that the quasiparticle energy dispersion is linear in all directions near the bulk nodal point. Furthermore, each band must be doubly degenerate because of the presence of both TRS and inversion-gauge symmetry. Therefore, the nodes are Dirac nodes.

Secondly, $\gamma_m = 1$ amounts to a Berry phase $\pm\pi$ in the decoupled mirror subspace with $s_x = \pm$. This implies a protected surface state at $(k_x = 0, k_y)$ for any $|k_y| < \pm k_n$ in any surface that preserves the mirror symmetry. Moreover, the presence of chiral symmetry in each mirror subspace pins the surface state to zero energy. Therefore, the Majorana arc must be dispersionless and spin degenerate.

From the above discussions, evidently, the combination of TRS, mirror symmetry, and inversion-gauge symmetry provides the protection of the Dirac nodes. When any of these symmetries is broken, the Dirac nodes become unstable. To facilitate the understanding of the consequence of symmetry breaking, we construct a local effective model near a Dirac node from general symmetry analysis. Since a Dirac node lies in a mirror invariant plane, the effective model must have the following *local* symmetries which commute with each other: chiral symmetry Π, mirror symmetry $\mathcal{M}$, and the product of TRS and inversion-gauge symmetry $\mathcal{W}$. For a Dirac node, the low-energy subspace has a dimension of four. We choose the representations of symmetry operations as follows: $\Pi = \tau_y$, $\mathcal{M} = -is_x$, and $\mathcal{W} = s_y\tau_z K$ with K the complex conjugation. Note that the Pauli matrices τ and s here have different meaning from

those in the original eight-band model (1). Under these symmetry constraints, the effective Hamiltonian takes the generic form of

$$H_D = k_x s_y \tau_x - k_y s_x \tau_x + k_z \tau_z. \qquad (7)$$

When the mirror symmetry is broken, the Dirac node loses its protection and thus may be gapped out. For example, a mirror symmetry breaking perturbation $\delta s_z \tau_x$
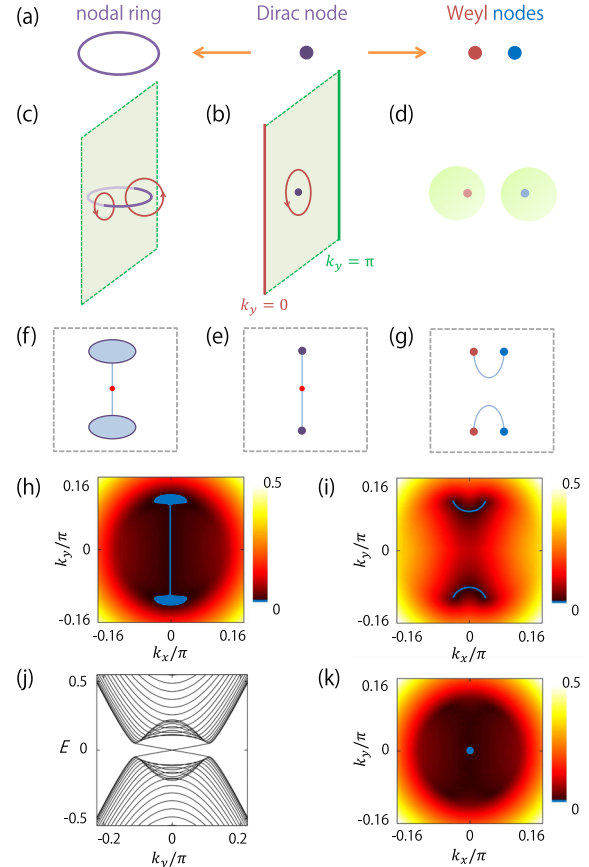
FIG. 2 (color online). Consequences of symmetry breaking for a Dirac SC. (a) When the inversion-gauge symmetry or TRS is broken, a Dirac node evolves into a nodal ring or two Weyl nodes normal to the mirror invariant plane, respectively. (b)–(d) A Dirac node (nodal ring) protected by the mirror (total) winding number ± 1 of the surrounding loop (red); a Weyl node protected by the Chern number ± 1 of the surrounding sphere (light green). (e)–(g) Sketches of the surface zero-energy states for each case. (e) Majorana Kramers arc (light blue) connecting the two surface projected Dirac nodes. (f) Two surface projected nodal rings with an extended area of zero-energy states inside. (g) A surface arc connecting a pair of surface projected Weyl nodes. (h)–(k) Tight binding calculations [33] for a (001) slab. (h) and (i) correspond to the scenarios in (f) and (g), respectively. (j) and (k) show that a Dirac SC may become a fully gapped topological SC when the mirror symmetry is broken. The blue color corresponds to the zero energy. We have chosen $\sigma_z\tau_z$ to break the inversion-gauge symmetry, $\sigma_x s_x$ to break TRS, and $\sigma_y s_z \tau_x$ to break the mirror symmetry, respectively.

in (7) leads to doubly-degenerate gapped Dirac bands with dispersion $\varepsilon = \pm\sqrt{k^2 + \delta^2}$. However, the Majorana Kramers pair is even robust against mirror symmetry breaking, as long as the perturbation does not close the gap along the time-reversal and mirror invariant line with nontrivial γ_m. This is because the parity of total γ_m determines [26] the $\mathbb{Z}_2$ index of a SC with TRS, and in the current example odd γ_m makes the $\mathbb{Z}_2$ index nontrivial. Therefore, breaking the mirror symmetry may gap the Dirac nodes producing a topological SC [26,28,37] for which the Majorana arc becomes the helical Majorana surface state, as seen in Figs. 2(j)–2(k).

When the inversion-gauge symmetry is broken, the nodal point is not required to be fourfold degenerate. Thus, the Dirac node splits into two doubly degenerate nodes in the mirror invariant plane, one in each mirror subspace. In this plane, γ_t and γ_m are ± 1 for any loop only enclosing one doubly degenerate node. Off this plane, even though γ_m can no longer be defined, γ_t is still well defined for any fully gapped loop since the chiral symmetry is unbroken. Evidently, the pair of nodes in the plane can extend off the plane and form a nodal ring, which has to be normal to the plane as required by TRS and mirror symmetry, as sketched in Fig. 2(c). For example, such a symmetry breaking term $\delta\tau_x$ in (7) leads to a spectrum $\varepsilon^2 = (\sqrt{k_x^2 + k_y^2} \pm \delta)^2 + k_z^2$, which contains a nodal ring normal to the mirror invariant plane. As a consequence at the surface respecting the mirror symmetry, the projected nodal ring has an extended area of zero energy modes inside [38–41] and there is a dispersionless and spin degenerate surface arc connecting the pair of rings, as shown in Figs. 2(f)–2(h).

A Dirac node may split into a pair of Weyl nodes only when TRS is broken. In the presence of chiral symmetry, any Chern number must be zero [26,42] and thus an isolated Weyl node cannot be protected. Indeed, the product of TRS and PHS is a chiral symmetry. Since PHS is intrinsic for any 3D SC, a Weyl node can only be protected when TRS is broken. As an example, a symmetry breaking term $\delta s_x \tau_y$ in (7) splits the Dirac node into two Weyl nodes with energy dispersion $\varepsilon = \pm\sqrt{(k_x \pm \delta)^2 + k_y^2 + k_z^2}$. When the mirror symmetry is unbroken, no node can be protected in the mirror invariant plane due to the absence of chiral symmetry, and thus the two Weyl nodes move off the plane normally in opposite directions. Once the pair of Weyl nodes splits in momentum instead of in energy, the inversion-gauge symmetry pins them to zero energy. These results, together with the symmetry breaking perturbations in the original $Cu_xBi_2Se_3$ model are described in Fig. 2.

All the above features are reminiscent of 2D and 3D Dirac semimetals [3–12], in which Dirac nodes are protected by sublattice symmetries and a set of crystalline constraints, respectively. Analogically, the nodal phase described by Eqs. (6) and (7) should be entitled "Dirac

SCs in 3D." When γ_m changes by N from $k_y = 0$ to π in the mirror invariant plane, a pair of nodal points with k^N dispersion appears and in general each node splits into N Dirac nodes. A rotational symmetry may dictate and relate multiple pairs of Dirac nodes, which can be obtained by applying Eq. (6) wherever applicable.

The form of surface Majorana arcs of a Dirac SC depends on the surface orientation. For example, in Fig. 1(f) the two bulk nodes project to the same point in the (010) surface BZ and the surface Majorana arcs shrink to a point, in sharp contrast to the case for (001) surface. The surface density of states [43] thus differs between the two surfaces, as shown in Fig. 1(g). At those surfaces breaking the mirror symmetry, the dispersionless surface arc becomes dispersive. Thus, to identify a nodal phase using surface sensitive probes, it is necessary to measure multiple surfaces with different orientations. Besides the appealing surface consequences, symmetry-protected pseudorelativistic physics occurs near each Dirac node, and chiral and axial anomalies [44,45] further arise when the Dirac node splits into a pair of Weyl nodes. The two anomalies may, respectively, lead to anomalous thermal (spin) Hall effect and anomalous angular momentum [45], manifesting the TRS breaking.

The 3D Dirac SCs may be realized in the nodal phase of $Cu_xBi_2Se_3$ [28] or the B phase of UPt_3 [46]. The former has served as a concrete example to illustrate the essential physics in this Letter, though its precise pairing symmetry is still under hot debate [28,47–63]. Recently, there is a hint of the existence of nodal points in the specific heat data of $Cu_xBi_2Se_3$ at high x values [64]. As suggested by our theory, different symmetry breaking in different samples may explain why different groups have observed different phases of $Cu_xBi_2Se_3$. The search for other candidate materials goes well beyond the scope here and deserves a separate study in the near future.

Note added.—Our criterion also suggests the possible existence of a third class of 3D Dirac semimetals [12], where a sublattice symmetry acts as the required chiral symmetry. The 3D Dirac and Weyl points were also found to exist in Andreev spectra at Josephson junctions [42]. Our criterion can also be used to search for Dirac and Weyl points in 2D systems that are mirror invariant planes.

*zhang@utdallas.edu

[1] M. Z. Hasan and C. L. Kane, Rev. Mod. Phys. **82**, 3045 (2010).

[2] X. Qi and S. Zhang, Rev. Mod. Phys. **83**, 1057 (2011).

[3] F. Zhang, B. Sahu, H. Min, and A. H. MacDonald, Phys. Rev. B **82**, 035409 (2010).

[4] F. Zhang, J. Jung, G. A. Fiete, Q. Niu, and A. H. MacDonald, Phys. Rev. Lett. **106**, 156801 (2011).

[5] S. M. Young, S. Zaheer, J. C. Y. Teo, C. L. Kane, E. J. Mele, and A. M. Rappe, Phys. Rev. Lett. **108**, 140405 (2012).

[6] Z. Wang, Y. Sun, X. Q. Chen, C. Franchini, G. Xu, H. Weng, X. Dai, and Z. Fang, Phys. Rev. B **85**, 195320 (2012).

[7] Z. Wang, H. Weng, Q. Wu, X. Dai, and Z. Fang, Phys. Rev. B **88**, 125427 (2013).

[8] J. A. Steinberg, S. M. Young, S. Zaheer, C. L. Kane, E. J. Mele, and A. M. Rappe, Phys. Rev. Lett. **112**, 036403 (2014).

[9] M. Neupane, S. Xu, R. Sankar, N. Alidoust, G. Bian, C. Liu, I. Belopolski, T.-R. Chang, H.-T. Jeng, H. Lin, A. Bansil, F. Chou, and M. Z. Hasan, arXiv:1309.7892.

[10] S. Borisenko, Q. Gibson, D. Evtushinsky, V. Zabolotnyy, B. Buechner, and R. J. Cava, arXiv:1309.7978.

[11] Z. K. Liu, B. Zhou, Z. J. Wang, H. M. Weng, D. Prabhakaran, S.-K. Mo, Y. Zhang, Z. X. Shen, Z. Fang, X. Dai, Z. Hussain, and Y. L. Chen, arXiv:1310.0391.

[12] B.-J. Yang and N. Nagaosa, arXiv:1404.0754.

[13] S. Murakami, New J. Phys. **9**, 356 (2007).

[14] X. Wan, A. M. Turner, A. Vishwanath, and S. Y. Savrasov, Phys. Rev. B **83**, 205101 (2011).

[15] A. A. Burkov, and L. Balents, Phys. Rev. Lett. **107**, 127205 (2011).

[16] A. A. Zyuzin, S. Wu, and A. A. Burkov, Phys. Rev. B **85**, 165110 (2012).

[17] C. Fang, M. J. Gilbert, X. Dai, and B. A. Bernevig, Phys. Rev. Lett. **108**, 266802 (2012).

[18] E. B. Kolomeisky and J. P. Straley, arXiv:1205.6354; arXiv:1210.1803; E. B. Kolomeisky, J. P. Straley, and H. Zaidi, Phys. Rev. B **88**, 165428 (2013).

[19] H. Lin and S.-T. Yau, Int. J. Mod. Phys. B **27**, 1350107 (2013).

[20] G. E. Volovik, *The Universe in a Helium Droplet* (Clarendon Press, Oxford, 2003); JETP Lett. **93**, 66 (2011).

[21] T. Meng and L. Balents, Phys. Rev. B **86**, 054504 (2012).

[22] J. D. Sau and S. Tewari, Phys. Rev. B **86**, 104509 (2012).

[23] T. Das, Phys. Rev. B **88**, 035444 (2013).

[24] Y. Xu, R. Chu, and C. Zhang, arXiv:1310.4100.

[25] P. Goswami and L. Balicas, arXiv:1312.3632.

[26] F. Zhang, C. L. Kane, and E. J. Mele, Phys. Rev. Lett. **111**, 056403 (2013).

[27] H. Yao and S. Ryu, Phys. Rev. B **88**, 064507 (2013).

[28] L. Fu and E. Berg, Phys. Rev. Lett. **105**, 097001 (2010).

[29] F. Zhang, C. L. Kane, and E. J. Mele, Phys. Rev. B **86**, 081303(R) (2012).

[30] C.-X. Liu, X.-L. Qi, H. J. Zhang, X. Dai, Z. Fang, and S.-C. Zhang, Phys. Rev. B **82**, 045122 (2010).

[31] F. Zhang, C. L. Kane, and E. J. Mele, Phys. Rev. Lett. **111**, 056402 (2013).

[32] R. Jackiw and C. Rebbi, Phys. Rev. D **13**, 3398 (1976).

[33] Here we use $v = 1.5$, $v_z = 1$, $m = 0.8$, $\mu = 1$, and $\Delta = 0.2$. In Fig. 2(i), we take $m = 0$ and $\mu = 0.4$ for better visualization.

[34] Q.-H. Wang, D. Wang, and F.-C. Zhang, Phys. Rev. B **81**, 035104 (2010).

[35] A small regularization ($\propto k^2$) is needed in the mass term to recover the trivial vacuum state at $k = \infty$.

[36] At $k_y = \pi$ the gap must be trivial and adiabatically connected to the vacuum state.

[37] M. Sato, Phys. Rev. B **81**, 220504(R) (2010).

[38] A. P. Schnyder and S. Ryu, Phys. Rev. B **84**, 060504(R) (2011).

[39] P. M. R. Brydon, A. P. Schnyder, and C. Timm, Phys. Rev. B **84**, 020501(R) (2011).

[40] B. Beri, Phys. Rev. B **81**, 134515 (2010).

[41] M. Sato, Y. Tanaka, K. Yada, and T. Yokoyama, Phys. Rev. B **83**, 224511 (2011).

[42] F. Zhang and C. L. Kane, Phys. Rev. B **90**, 020501(R) (2014).

[43] A. Yamakage, K. Yada, M. Sato, and Y. Tanaka, Phys. Rev. B **85**, 180509(R) (2012); S. Takami, K. Yada, A. Yamakage, M. Sato, and Y. Tanaka, arXiv:1402.4898.

[44] C.-X. Liu, P. Ye, and X.-L. Qi, Phys. Rev. B **87**, 235306 (2013).

[45] M. N. Chernodub, A. Cortijo, A. G. Grushin, K. Landsteiner, and M. A. H. Vozmediano, Phys. Rev. B **89**, 081407(R) (2014).

[46] Y. Tsutsumi, M. Ishikawa, T. Kawakami, T. Mizushima, M. Sato, M. Ichioka, and K. Machida, J. Phys. Soc. Jpn. **82**, 113707 (2013).

[47] Y. S. Hor, A. J. Williams, J. G. Checkelsky, P. Roushan, J. Seo, Q. Xu, H. W. Zandbergen, A. Yazdani, N. P. Ong, and R. J. Cava, Phys. Rev. Lett. **104**, 057001 (2010).

[48] L. A. Wray, S. Xu, Y. Xia, Y. Hor, D. Qian, A. Fedorov, H. Lin, A. Bansil, R. J. Cava, and M. Z. Hasan, Nat. Phys. **6**, 855 (2010).

[49] L. Hao and T. K. Lee, Phys. Rev. B **83**, 134516 (2011).

[50] M. Kriener, K. Segawa, Z. Ren, S. Sasaki, and Y. Ando, Phys. Rev. Lett. **106**, 127004 (2011).

[51] P. Das, Y. Suzuki, M. Tachiki, and K. Kadowaki, Phys. Rev. B **83**, 220513 (2011).

[52] M. Kriener, K. Segawa, Z. Ren, S. Sasaki, S. Wada, S. Kuwabata, and Y. Ando, Phys. Rev. B **84**, 054513 (2011).

[53] S. Sasaki, M. Kriener, K. Segawa, K. Yada, Y. Tanaka, M. Sato, and Y. Ando, Phys. Rev. Lett. **107**, 217001 (2011).

[54] T. Kirzhner, E. Lahoud, K. B. Chaska, Z. Salman, and A. Kanigel, Phys. Rev. B **86**, 064517 (2012).

[55] T. V. Bay, T. Naka, Y. K. Huang, H. Luigjes, M. S. Golden, and A. de Visser, Phys. Rev. Lett. **108**, 057001 (2012).

[56] X. Chen, C. Huan, Y. S. Hor, C. A. R. Sá de Melo, and Z. Jiang, arXiv:1210.6045.

[57] B. J. Lawson, Y. S. Hor, and L. Li, Phys. Rev. Lett. **109** 226406 (2012).

[58] T. H. Hsieh and L. Fu, Phys. Rev. Lett. **108**, 107005 (2012).

[59] H. Peng, D. De, B. Lv, F. Wei, and C.-W. Chu, Phys. Rev. B **88**, 024515 (2013).

[60] N. Levy, T. Zhang, J. Ha, F. Sharifi, A. A. Talin, Y. Kuk, and J. A. Stroscio, Phys. Rev. Lett. **110**, 117001 (2013).

[61] T. Kondo, Y. Nakashima, Y. Ota, Y. Ishida, W. Malaeb, K. Okazaki, S. Shin, M. Kriener, S. Sasaki, K. Segawa, and Y. Ando, Phys. Rev. Lett. **110**, 217601 (2013).

[62] B. Zocher and B. Rosenow, Phys. Rev. B **87**, 155138 (2013).

[63] S.-K. Yip, Phys. Rev. B **87**, 104505 (2013).

[64] Y. Ando (private communication).